RSC Advances

ROYAL SOCIETY OF CHEMISTRY

www.rsc.org/advances

Composition-controlled synthesis of $Li_xCo_{3-x}O_4$ solid solution nanocrystals on carbon and their impact on electrocatalytic activity toward oxygen reduction reaction

Jingjun Liu, Hongcan Liu, Feng Wang*, Ye Song

State Key Laboratory of Chemical Resource Engineering, Beijing Key Laboratory of Electrochemical Process and Technology for Materials, Beijing University of Chemical Technology, Beijing 100029, China. E-mail: wangf@mail.buct.edu.cn; Fax: +86 10 64451996; Tel: +86 10 64451996

Abstract:

Through incorporation of other metal element like Li, K and Cu into Co_3O_4 lattice, tuning electronic structures of carbon-supported Co_3O_4 may be an effective way to improve electrochemical properties of the oxide as an efficient catalyst for the oxygen reduction reaction (ORR). In this paper, we have synthesized Li-doped Co_3O_4 (Li/Co=0, 2.5%, 5%, 7.5%) solid solution nanocrystals through direct nucleation and growth of the lithium-colbat oxide on a acid-treated carbon black. The carbon supports $Li_xCo_{3-x}O_4$ spinel nanocrystals with average particle size of approximately 4 nm, covered evenly on the surface of carbon in this hybrid. The electrocatalysis experiments in an alkaline solution reveal a close correlation between the ORR electrocatalytic activities and the doped Li contents of these $Li_xCo_{3-x}O_4$/C catalysts. Interestingly, the half-wave potential and the mass-specific activity of these catalysts show a typical volcano plot as a function of Li contents. Among all the synthesized $Co_{3-x}O_4$/C samples, the sample prepared at the Li/Co atomic ratio of 5% displays the most positive half-wave potentail and the largest mass-specific activity respectively, which are 70mV and 3.3 times higher than the undoped Co_3O_4/C. Comapared with that of the undoped Co_3O_4/C, the remarkly increased content of covalent O=C–O–Co^{III}–O bonds formed at the interfaces between Li-doped Co_3O_4 and carbon support is responsible for the improved electro-catalytic performances of the doped catalyst. Moreover, the covalent electron transfer from the Co^{III} species to the electron-withdrawing O=C–O species through the O=C–O–Co^{III}–O bonds can not only promote the oxidation of active sites Co^{III} into Co^{IV} but also facilitate the surface hydroxide displacement, which can significantly contribute to the ORR kinetics. Therefore, the exact understanding of the unique interfacial electronic structures of the $Li_xCo_{3-x}O_4$/C hybrids is very important to develop the lithium-colbat oxides on carbon as next-generation catalysts for ORR.

Keywords: lithium-colbat oxides, carbon black, Li content, oxygen reduction reaction, electronic structure

1. Introduction

In recent years, transition metal oxides with a spinel structure (AB_2O_4, A, B=metal) have been considered as efficient electro-catalysts for oxygen reduction reaction (ORR) in alkaline environment because of their low cost, high catalytic activity and high durability. [1-2] As far as we known, the spinel structure is built around a closely packed array of O^{2-} ions, along with A^{2+} and B^{3+} cations occupying respectively part or all of the tetrahedral and octahedral sites. [3] Moreover, mixed valence oxides of transition metals like Co_3O_4 and Mn_3O_4, in which A^{2+} and B^{3+} cations belong to one element, are one of the most important categories of the spinel oxides that exhibit relatively high ORR catalytic activity in alkaline conditions. [4] It is reported that Co_3O_4 and Mn_3O_4 spinel nanocrystals supported on carbon supports like carbon black, carbon nanotubes, carbon nanoweb and graphene as hybrid materials have been developed and their electro-catalytic activities toward the ORR are comparable with that a commercial Pt/C (E-TEK). [5-7]

By now, the carbon-supported spinel oxides like Co_3O_4 have been considered to one of the most promising ORR electrocatalysts as a potential alternative to Pt/C in the alkaline environments. [5] However, the practical application of the carbon-supported Co_3O_4 as electrocatalysts for ORR is prevented due to their unsatisfactory electronic conductivities, low mass-specific activity, and large volume expansion, which is caused by the valence variation of cobalt ions through charge/discharge during the electrochemical reaction. [8] To overcome these issues, it is necessary to increase the electrode loading of Co_3O_4 on carbon as much as possible due to its low mass-specific activity that involved with the relatively low active specific surface of cobalt-based spinel oxide for oxygen reduction, compared with Pt-based catalysts. However, a little increase of the electrode loadings will also remarkably decline the ORR activity of the oxide due to its increasing resistivity. [9]Moreover, large volume expansion may lead to the weakness of the force among the ions, which will result in electrocatalysts pulverization. [10] These

disadvantages above seriously hinder the application of Co_3O_4/C hybrid catalysts as the next generation electrocatalysts. Thus, it is highly desirable to develop modified spinel oxide catalysts for the ORR through decreasing the electronic and ionic resistivity and/or increasing the mass-specific activity of the oxide. [11]

It is believed that the integration of other metal elements such as Li, K and Cu into a spinel oxide matrix may be a promising way to enhance the electrochemical performance of the oxide.[12-18] After the integration of these metal elements, a spinel oxide-based solid solution can be achieved, which keeps the structure of the oxide matrix. The reasons for the improved activity of these doped oxides can be explained as following. On the one hand, it is believed that the doping of secondary metal elements like Li^+ and K^+ into the cobalt oxide increases the amount of dislocations and imperfections in the spinel Co_3O_4 crystal structure, which enable the transition of the electrons to take place easily. Thus, the conductivity of the doped Co_3O_4 is significantly increased. [12, 13] On the other hand, the doping of monovalent cations such as Li^+ and K^+ also increase the amount of Co^{3+} cations, which is the active sites of the cobalt oxide, relative to the Co^{2+} cations, as a result of the charge balance in this oxide. Liu and his co-workers [19] reported that a partial substitution of cobalt ions by foreign Li^+ ions in Co_3O_4 to form a newly $Li_xCo_{3-x}O_4$ phase can remarkably enhances the intrinsic oxygen reduction activities of the oxide. They further confirmed that lithium ions doped in the cobalt oxide will occupy the tetrahedral sites where the Co^{2+} cations occupied, which leads to that the amount of Co^{2+} cations is decreasing, and the amount of Co^{3+} cations is increasing in the tetrahedral sites to compensate the charge of Li^+. Moreover, it is believed that the incorporation of other metal elements into Co_3O_4, such as Li^+, Cu^{2+} and Mn^{2+} ions, obtains a greater electrochemically active surface area than pure Co_3O_4, thereby which can enhance the mass-specific activity of Co_3O_4. [17, 18] In addition, through doping Li ions, these Li ions with very small size may facilitate the alleviation of the mechanical stress induced by volume changes of the oxide during repeated charge/discharge cycles. It can avoid the possible pulverization of the cobalt oxide nanoparticles caused by volume expansion of the oxide during the ORR. Recently, Manthiram et al. [20] have synthesized chemically delithiated spinel $Li_{1-x}CoO_2$ samples through chemically extracting lithium from $LiCoO_2$, which consisted of the cubane-like cubic Co_4O_4 units. The results of the chemically extracting lithium were that a part of the Co^{3+} ions were oxidized to Co^{4+} and created mixed-valent Co^{3+}/Co^{4+} ions: 3d energy with the top of the O^{2-}: 2p band, which contributed to the high activities of these delithiated composition. This finding further confirms the spinel lithium cobalt oxides can be a kind of efficient electrocatalysts for oxygen reduction reaction. Thus, the integration of Li into a spinel oxide matrix to form spinel oxide-based solid solutions may be an effective way to improve the electrochemical performances of the oxide on carbon. Despite the origin of the improved activity of these oxide-based catalysts for the ORR is still debated, it is believed that the ORR activity mainly results from three aspects: the active transition metal oxides, doped carbon support, and synergistic effects between them. There are many previous works reported that the oxides exhibited effective activities during ORR[21, 22] while other papers purported that the carbon materials with N-doped or B-doped exhibited high activities during ORR[23, 24]. However, they ignored that if the oxides are supported on the carbon, the synergistic interaction between the oxide and the carbon supports may play a key role in the catalysis of ORR. As reported in the literature, [25, 26] there are chemical interaction (such as noncovalent or covalent bonding) at the interface between the oxides and their carbon substrates, which can lead to strong synergistic effects that dominate the ORR kinetics. However, the nature of the synergistic effect at the interface between the inexpensive transition oxide and carbon support remain unclear, since the exact structure of the interface has been paid less attentions. To ignore the synergistic effect may literally close the door to advancement in this field, because the studying of the synergistic effect can offer an opportunity to deeply reveal ORR mechanism catalyzed by these catalysts. Thus, the really fundamental understanding of the ORR kinetics is helpful to develop highly active and economical non-noble metal composites as next-generation catalysts for the ORR.

In this work, we prepared the carbon-supported $Li_xCo_{3-x}O_4$ solid solution with different Li contents (atomic ratio of Li/Co=0%, 2.5%, 5%, 7.5%) via the in-situ nucleation and growth of the solid solution nanoparticles on an acid-treated carbon black with a simple hydrothermal method. The electrocatalytic activities of the carbon-supported $Li_xCo_{3-x}O_4$ solid solutions were characterized using rotating electrode in alkaline solutions to elucidate the close correlation of the improved ORR performances as a function of the Li contents. X-ray photoelectron spectroscopy (XPS) and FT-IR were carried out on the hybrid catalysts in order to investigate the unique electronic interactions at the interfaces between Li-doped Co_3O_4 and carbon support in their hybrids. The aim of the work is to gain insights into the intrinsic

correlation between the improved activity enhancement and the electronic structures in the hybrid catalysts. This information is important for understanding the physical origin of the activity of $Li_xCo_{3-x}O_4$/C catalysts during the ORR.

2. Experimental section

2.1 Materials synthesis

The carbon-supported $Li_xCo_{3-x}O_4$ solid solutions fabricated at different Li contents were prepared with hydrothermal method via a direct nucleation and growth of these Li-doped cobalt oxide nanocrystals on a carbon black (Vulcan XC-72, Cabot Corporation). Prior to the synthesis of carbon-supported $Li_xCo_{3-x}O_4$ ($Li_xCo_{3-x}O_4$/C), the carbon was pre-treated by stirring at 120 °C in a concentrated nitric acid (HNO_3) for 10 h, and then washed with ultrapure water until the pH becomes neutral. Subsequently, carbon-supported $Li_xCo_{3-x}O_4$ solid solution was synthesized via hydrothermal reaction method in an ethanol system. In a typical experiment, 0.13 mmol cobalt acetate tetrahydrate ($(Co(Ac)_2{\cdot}4H_2O)$, 21 mg treated Vulcan XC-72, and different quantities of lithium acetate dehydrate ($(Li(Ac){\cdot}2H_2O$, atomic ratios of Li/Co were 0%, 2.5%, 5%, 7.5%) were dissolve in 30 ml mixing solution about ethanol, deionized water and ammonia. Then, the mixture was refluxed in an oil bath under stirred at 80℃ for 10h, then cooled naturally. Following, the reaction mixture was transferred to an autoclave for hydrothermal reaction at 150℃ for another 3h. The resulted product was collected by centrifugation and washed with ethanol and water, followed by drying at 80 °C for 24 h.

2.2 Characterization

The $Li_xCo_{3-x}O_4$/C hybrid samples with different Li contents were characterized with high-resolution transmission electron microscopy (HRTEM, JEOL JMS-2100 microscope), X-ray diffraction (XRD, D/max 2500 X-ray powder diffraction analyzer with Cu Kα radiation radiation of wavelength 0.15406 nm), Raman spectroscopy (LabRam HR800 Raman spectroscopy analyzer), X-ray photoelectron spectroscopy (XPS, Thermo ESCALAB 250 X-ray photoelectron spectroscopy analyzer) and Fourier-transform infrared spectroscopy (FT-IR, MAGNA-IR 750 FT-IR spectrometer) using a KBr-disc method. On the XPS patterns, all binding energy values were calibrated to the C1s signal which was set at 284.6eV.

2.3 Electrochemical measurements

The electrochemical experiments were carried out on a rotating disk electrode device (AFCBP1 type, PINE, USA), in 1M NaOH solution and 0.5M H_2SO_4 utilizing a three electrode system consisting of a saturated calomel electrode (SCE) as the reference, a platinum wire as the counter electrode and a $Li_xCo_{3-x}O_4$ /C power coated glassy carbon electrode (S=0.247 cm^2) as the working electrode. The working electrode was prepared as follows: Five milligrams of these $Li_xCo_{3-x}O_4$/C samples was dispersed by sonication for 30 min in a mixture of ethanol (1 ml) and Nafion solution (50 µl, 5 wt.%) (DuPont, USA). After sonication, 20 µl of the solution was transferred onto the glassy carbon electrode and dried at room temperature. Before the test, the electrolytic solution was saturated with pure oxygen. And during measurements, a constant gentle flow of O_2 was bubbled through the electrolyte solution to ensure continuous O_2 saturation. And the scan rate used for all measurements was 5mV/s.

3. Results and discussion

3.1 Fabrication of $Li_xCo_{3-x}O_4$ solid solution nanoparticles on carbon.

Figure 1 shows the HRTEM images of the carbon-supported Li-doped Co_3O_4 nanoparticles fabricated at different Li/Co atomic ratios (0%, 2.5%, 5%, 7.5%). As observed, the Li-doped Co_3O_4 nanocrystals are uniformly dispersed on the surfaces of the carbon black matrix. The average diameter of these nanoparticles fabricated at different Li contents is approximately 4 nm with a narrow particle size distribution, revealing little impact of the added lithium contents on the size of the Co_3O_4. Figure 2A shows the characteristic XRD patterns of these samples. Apart from the peak (at ～26°) observed in the XRD diffraction lines originated from carbon support, these samples exhibit XRD patterns identical to pure Co_3O_4 sample, as shown in Figure 2A. The peaks at 19° , 31° , 37° , 45° , 59° and 65° are assigned to the (111), (220), (311), (400), (511) and (440) planes of Co_3O_4 phase with a spinel structure (space group Fd3m), consistent with JCPDS Card File no. 43-1003. In Figure 1, the larger gray particles are carbon supports, and the dark spherical particles anchoring the carbon supports should be $Li_xCo_{3-x}O_4$, since

heavy metal oxides usually present strong contrast against the background. In addition, the particles that show a typical, apparent and grid-like lattice fringe are $Li_xCo_{3-x}O_4$ particles, while the particles that only show simple parallel lattice fringe are carbon supports. As evidenced from HRTEM in Figure 1(insets), lattice fringes of these Li-doped Co_3O_4 samples have interplanar spacings of 0.28nm, agreeing well with the (220) lattice planes of the Co_3O_4. There are no extra peaks associated with impurities, such as pure Li or its oxides, were detected by XRD, indicating the possible formation of solid solution $Li_xCo_{3-x}O_4$ after Li insertion. But, no obvious peak shift is observed in these XRD lines for the synthesized $Li_xCo_{3-x}O_4$/C samples along with the increase in the Li contents, which is may for the reason that the size of Li^+ ions is small, relative to the Co^{2+} and Co^{3+} ions in the Co_3O_4 matrix.

To further confirm the formation of the $Li_xCo_{3-x}O_4$ solid solution nanocrystals on carbon, Raman scattering were conducted for the synthesized samples above, as depicted in Figure 2B. For these Li-doped Co_3O_4/C samples, five characteristic peaks in the Raman scattering line are observed at 189, 472, 509, 601 and 675 cm^{-1}, which corresponds respectively to the F^1_{2g}, E_g, F^2_{2g}, F^3_{2g} and A^1_g symmetric phonon modes of crystalline Co_3O_4. [27] In addition, the A^1_g peak in Raman spectra of these Li-doped Co_3O_4/C catalysts shifts to higher frequency relative to the pure Co_3O_4/C. Moreover, with an increase in the contents of Li atoms, the offset of A^1_g the recorded peak increases gradually. It is believed that the A^1_g mode is associated with the oxygen motion in the spinel oxide, and the newly formed crystalline lattice defects and disorder obtained by addition of other second element into the oxide have an impact on the oxygen motion. [28] Based on this suggestion above, we can conclude that the obvious shift of the A^1_g peak for the Li-doped Co_3O_4 samples implies that Co sites in Co_3O_4 are substituted by the added Li^+ and then generate new crystalline lattice defects and disorder, thereby forming a $Li_xCo_{3-x}O_4$ continuous solid solution on carbon.

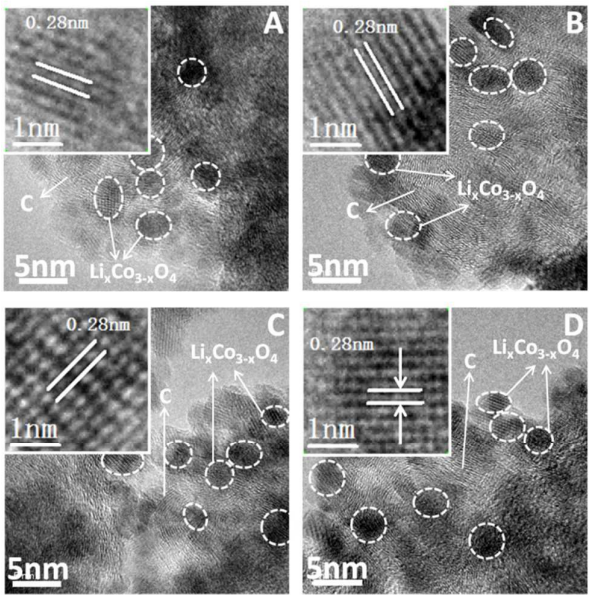

Figure 1. HRTEM images of the synthesized $Li_xCo_{3-x}O_4$/C samples fabricated at different Li/Co atomic ratios (0%, 2.5%, 5%, 7.5%).

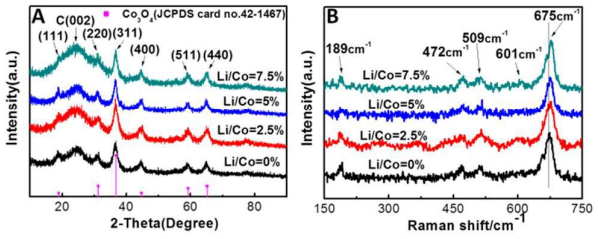

Figure 2. (A) XRD spectra of the $Li_xCo_{3-x}O_4$/C samples fabricated at different Li/Co atomic ratios (B) Raman spectra of the $Li_xCo_{3-x}O_4$/C samples above.

For purpose of further verifying that Li integrate into the lattice of Co_3O_4, we annealed the Li-doped Co_3O_4/C (Li/Co=5%) sample at 500℃ in an argon atmosphere. Figure 3A shows the XRD patterns of the Li-doped Co_3O_4/C samples and the sample after annealing. After the annealing, the XRD pattern can be exactly indexed to the pure CoO phase (JCPDS card no.43-1004) without any impurities, apart from the peak (at ~26°) observed in the XRD diffraction lines originated from carbon support. This result reveals that the Lithium (Li) has not evaporated separately in the form of Li_2O, but exists in the solid solution and is limited in the lattice of Co_3O_4.[8] Rasiyah [29] suggested that in $Li_xCo_{3-x}O_4$ solid solution, Li^+ may enter into the tetrahedral sites and the extra charge was compensated by additional Co^{3+} in the tetrahedral sites, which was described as $[(Li^+_xCo^{2+}_{1-2x}Co^{3+}_x)_A(Co^{3+}_2)_BO_4]$. However, Nikolov [30] argued that Li^+ may enter into the octahedral sites and the extra charge was compensated by excess Co^{4+} in the octahedral sites, which was described as $[(Co^{2+}_1)_A(Li^+_xCo^{3+}_{2-x}Co^{4+}_x)_BO_4]$. Nikolov further reported that the distribution of Li^+ ions in the tetrahedral or octahedral sites of the Co_3O_4 spinel lattice was influenced by the synthesis temperature and the Li^+ was inclined to enter into the octahedral sites at high reaction temperatures in air atmosphere. In our case, the low reaction temperature 150℃ was afforded during the fabrication procedure (seen the Experimental section),which makes these added Li^+ ions preferentially enter tetrahedral sites rather than the octahedral sites in the Co_3O_4 lattices. The occupying of Li^+ ions in tetrahedral sites would lead to the remarkable increase of Co^{3+} in the prepared Li-doped Co_3O_4 spinel structure. The schematic illustration of the as-synthesized Li-doped Co_3O_4 spinel structure is shown in Figure 3B. Based on the results in the literature, [12, 13, 29] since Co^{3+} is the active site of Co_3O_4 for the ORR, the additional Co^{3+} ions in the Li-doped Co_3O_4 spinel structure as a result of Li ions incorporation maybe contribute the ORR kinetics over the Li-doped catalysts.

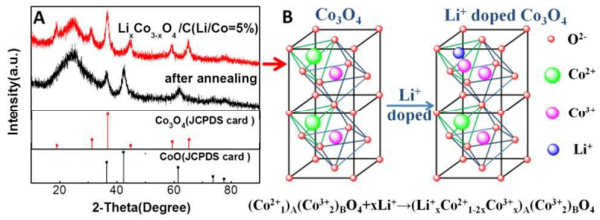

Figure 3. (A) XRD pattern of $Li_xCo_{3-x}O_4$/C(Li/Co=5%) sample and the sample after annealing at 500℃ in an argon atmosphere. (B) The schematic illustrate of Li doping into the spinel structure of Co_3O_4.

3.2 Chemical interaction between Li-doped Co_3O_4 and carbon in the hybrids

To further elucidate chemical interaction between the Li-doped Co_3O_4 nanocrystals and carbon support, we have explored the electronic structures at the interfaces in the hybrids. We employed X-ray photoelectron spectroscopy (XPS) to examine the electronic states of oxygen, carbon and Co atoms in the synthesized $Li_xCo_{3-x}O_4$/C (Li/Co=0, 2.5%, 5%, 7.5%) hybrids. The fitted O1s spectra in these Li-doped Co_3O_4/C samples display six peaks, as shown in Figure 4A. Two peaks 531.88eV, 533.87eV are assigned to the oxygen atoms connected to carbon atoms in C–O, O–C=O bonds, respectively. [31] Other three peaks at 529.89 eV, 531.23 eV and 532.67eV are ascribed to lattice oxygen (O^{2-}), surface-adsorbed oxygen (O_2^-) groups and OH^- group, [32-34] which are consistent with the results of the pure Co_3O_4/C. The last one at about 530.93 eV is attributed to the formation of the –O–Li bonds in the hybrid.[12] The content of the covalent O–C=O bonds as a function of the different Li contents in these hybrids is shown in Figure 4B. As observed, we can see that the incorporation of Li into Co_3O_4 lattice increased the content of the bond of O–C=O, compared with that of undoped Co_3O_4/C sample. Moreover, for the Li-doped samples, with increasing Li contents, the content of the covalent O–C=O bonds increase first and then decrease. For the catalyst prepared at the Li/Co atomic ratio of 5%, the content of the bond is up to 11.89%, which is much higher than the other $Li_xCo_{3-x}O_4$/C hybrids and pure Co_3O_4/C. Thus, It is concluded that the incorporation of Li element into Co_3O_4 lattice substantially promotes the formation of the O–C=O bonds for these $Li_xCo_{3-x}O_4$/C hybrids.

To further confirm the formation of the O–C=O bonds in these $Li_xCo_{3-x}O_4$/C samples, the C1s peaks of them have been determined and the obtained results are shown in Figure 4C. The C1s peaks of these samples could be fitted to three components at binding energies of 284.8eV, 286.3eV, 288.6eV, generally attributed to C-C, C-O, and O-C=O.[35,36] Through analyzing the amount of O–C=O, as shown in Figure 4D, we also can conclude that the doping of Li into Co_3O_4 lattice contribute to form the O–C=O bonds. Moreover, with increasing the Li contents, the content of the bond of O–C=O increase first and then decrease, and the highest content is observed for the sample prepared at the Li/Co atomic ratio of

5%. This result is in good agreement with the result of the O1s spectra shown in Figure 4B. Based on the fact of the increased ratio of Co^{3+}/Co^{2+} in the $Li_xCo_{3-x}O_4$/C hybrids shown in Figure 3, the increased O–C=O bonds may be associated to the O=C–O–Co^{III}–O bonds formed at the interface between Li-doped Co_3O_4 and carbon support.

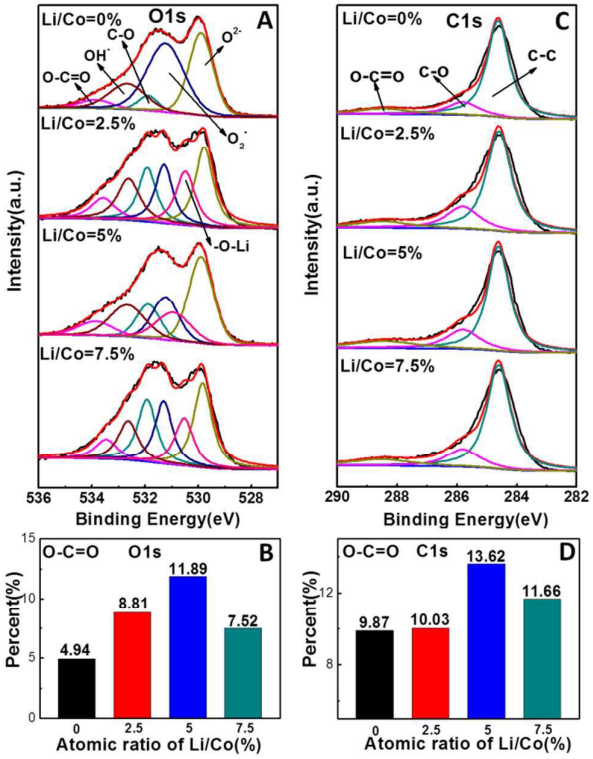

Figure 4. (A) XPS O1s spectra for the $Li_xCo_{3-x}O_4$/C samples fabricated at different Li/Co atomic ratios (0, 2.5%, 5%, 7.5%); (B) Contents of O-C=O bonds in the $Li_xCo_{3-x}O_4$/C samples, respectively; (C) XPS C1s spectra for the $Li_xCo_{3-x}O_4$/C samples; (D) Contents of O-C=O bonds in the $Li_xCo_{3-x}O_4$/C samples, respectively.

To confirm this assume, we further analysis the characteristic Co2p spectra for these $Li_xCo_{3-x}O_4$/C samples, as depicted in Figure 5 A～D. The obtained Co2p spectra consist of two main $Co2p_{1/2}$, $Co2p_{3/2}$, spin-orbit lines, at 795.2eV and 780.3eV, separated by about 15eV. Furthermore, two satellites located at approximately 10 eV above the primary binding energy peaks are detected, which is the characteristic of cobalt atoms in a cobalt oxide with Co_3O_4 stoichiometry.[37] All these spectra can be deconvoluted into two spin-orbit doublets: Do1 and Do2, and three satellite peaks: Sa1, Sa2 and Sa3, as depicted by Figure 5A～D. The peaks of Do1 ($Co2p_{3/2}$), Do1 ($Co2p_{1/2}$), Do2 ($Co2p_{3/2}$), Do2 ($Co2p_{1/2}$), Sa1, Sa2 and Sa3, are separately located at 779.7, 794.8, 781.1, 796.60, 784.4, 789.10, 803.92eV. [38, 39]The first spin-orbit doublet (Do1), the first satellite peak (Sa1) and the second satellite peak (Sa2) are associated with the octahedral Co^{3+} component of Co_3O_4. The second spin-orbit doublet (Do2) and the third satellite peak (Sa3) are characteristics of the tetrahedral Co^{2+} component of Co_3O_4. [40] Therefore, we calculate the Co^{3+}/Co^{2+} ratio through the XPS relative intensities corresponding to Co^{3+} and Co^{2+} ions. The result is shown in Figure 5E. As observed, after incorporation of Li^+, the Co^{3+}/Co^{2+} ratio almost increased. And the Co^{3+}/Co^{2+} ratio increase first and then decrease, with the increase in Li contents. The Co^{3+}/Co^{2+} ratio is max at 5% and the ratio is 1.14, which is obviously bigger than that of undoped Co_3O_4/C. Since Co^{3+} ions would act as donor and/or acceptor, which can capture and donate electrons during oxygen reduction reaction, [21] the ORR is assumed to take place at the active sites that are Co^{3+} ions with a higher oxidation state in the cobalt oxide. Thus, the increased Co^{3+} ions contribute to the ORR on the hybrid materials. More importantly, for the synthesized $Li_xCo_{3-x}O_4$/C hybrids, we find that the Co^{3+}/Co^{2+} ratios are in accord with contents the O–C=O bonds shown in Figure 4, revealing the formation of the O=C–O–Co^{III}–O bonds in this hybrid series. The atomic structure scheme of the covalent O=C–O–Co^{III}–O bonds at the interfaces between Li-doped Co_3O_4 and carbon support is shown in Figure 6. The formation of the unique

covalent bonds maybe contributes the ORR electro-catalytic activity of these hybrids as a result of covalent electron transfer across the interfaces.

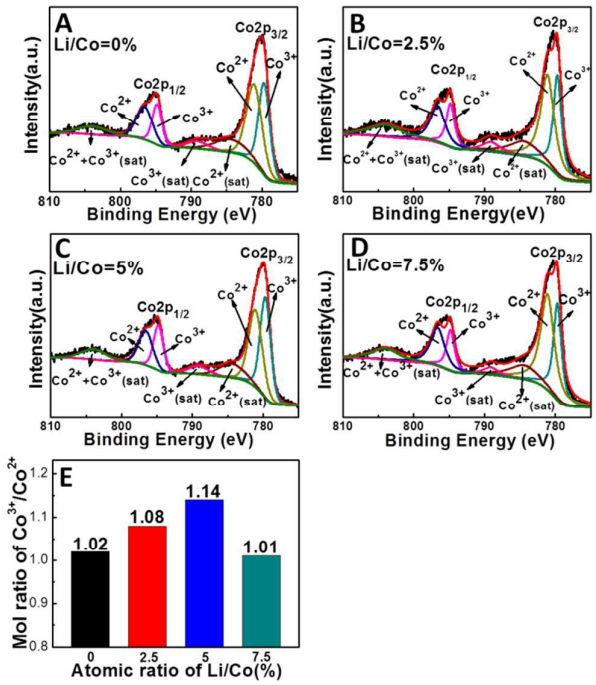

Figure 5. (A), (B), (C) and (D) XPS Co2p spectra for the $Li_xCo_{3-x}O_4$/C samples fabricated at different Li/Co atomic ratios (0, 2.5%, 5%, 7.5%); (E) the mol ratio of Co^{3+}/Co^{2+} in the $Li_xCo_{3-x}O_4$/C samples, respectively.

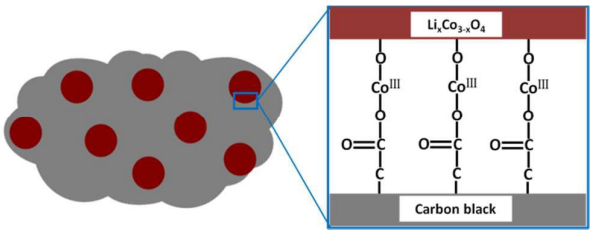

Figure 6. The schematic illustrating the typical interfacial structure of the synthesized $Li_xCo_{3-x}O_4$/C hybrid.

In order to reveal that the formation process of the covalent O=C–O–Co^{III}–O bonds at the interface between Li-doped Co_3O_4 and carbon support, we performed FT-IR to study the surface properties of the pure carbon black and $Li_xCo_{3-x}O_4$/C hybrid, as shown in Figure 7A. As we can see from Figure 7A, the pure carbon support shows several absorption bands at 3440 cm^{-1} (attributed to O-H stretching in water), 2924 and 2850 cm^{-1} (assigned to C-H stretching), 1721 cm^{-1} (assigned to stretching vibrations of carbonyl groups (-C=O) present in carboxyl or quinone groups), 1614 cm^{-1} (assigned to conjugated C=C stretching), 1397cm^{-1} (assigned to C-O stretching in carboxylate ions) and 1223 cm^{-1} (corresponding to C-O-H stretch in alcohols). [41, 42] However, for $Li_xCo_{3-x}O_4$/C (Li/Co=5%) hybrid, the two characteristic adsorption bands at 1721 cm^{-1} and 1223 cm^{-1}, respectively assigned to carboxyl or quinone groups and alcohols, disappear or become very weak after deposition of the Li-doped cobalt oxide on the carbon support. It reveals that there is no or very little carboxyl or quinone groups and alcohols existed on surface of the carbon component in the hybrid. Moreover, two new absorption bands at 671 cm^{-1} and 573 cm^{-1} (originating from the stretching vibrations of the Co-O bond) have been observed for the synthesized hybrid, which further confirm the deposition of the oxide onto the carbon. [43]

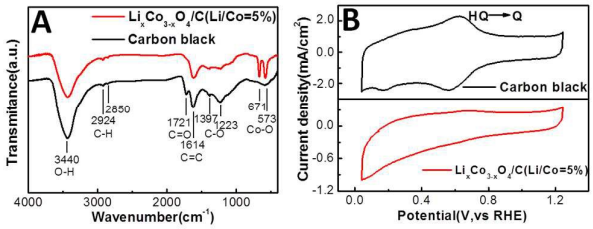

Figure 7. (A) FT-IR spectras of the acid-treated carbon black (the carbon support) and the $Li_xCo_{3-x}O_4$/C sample fabricated at the Li/Co atomic ratios of 5%.（B）Cyclic voltammograms of the acid-treated carbon black (the carbon support) and the $Li_xCo_{3-x}O_4$/C sample fabricated at the Li/Co atomic ratios of 5% in 0.5M H_2SO_4 at scan rate of 50mV/s.

To further confirm the fact that there are quinone groups existed only on surface of the pure carbon support rather than the "carbon component" in the $Li_xCo_{3-x}O_4$/C sample, we have conducted cyclic voltammograms for the above two samples in 0.5M H_2SO_4 at scan rate of 50mV/s, and the obtained results are shown in Figure 7B. It can be seen that there is an obvious redox peak appeared at about 0.6V vs RHE on the cyclic voltammograms of the pure carbon support, which can be attributed to the hydroquinone-quinone (HQ-Q) redox couple on most carbon material surface.[44, 45] It further confirms that there are quinone groups existed on the pure carbon support. However, the similar HQ-Q redox peak is not observed for the $Li_xCo_{3-x}O_4$/C sample, as shown in Figure 7B. This finding is in agreement with results from the FT-IR measurement. Thus, we can conclude that there is no or very little quinone groups existed on surface of the carbon component in the $Li_xCo_{3-x}O_4$/C hybrid. The disappeared quinone groups may be associated with the chemical deposition of the oxide nanoparticles on the carbon, because quinone groups can offer active sites for the chemical deposition of the oxide. In this way, the quinone groups may play a key role in the formation the covalent O=C–O–Co^{III}–O bonds at the interfaces between Li-doped Co_3O_4 and carbon support in their hybrid. In other words, the presence of quinone groups on the carbon surface as bridge may contribute the formation the covalent O=C–O–Co^{III}–O bonds in our case.

3.3 The enhanced electro-catalytic activity for ORR on $Li_xCo_{3-x}O_4$/C hybrids

The correlation between Li contents in these $Li_xCo_{3-x}O_4$/C catalysts prepared at different Li/Co ratios (Li/Co= 0%, 2.5%, 5%, 7.5%) and their electrocatalytic activity for the ORR was explored by using a rotating disk electrode (RDE) at a fixed rotation rate of 1600 rpm in oxygen-saturated 1 M NaOH solution at room temperature. Figure 8A shows a series of Rotating disk electrode voltammogram for these $Li_xCo_{3-x}O_4$/C catalysts. At the same time, the activity of the commercial Pt/C catalyst (20 wt% of Pt, relative to carbon, E-TEK) was measured for comparison.

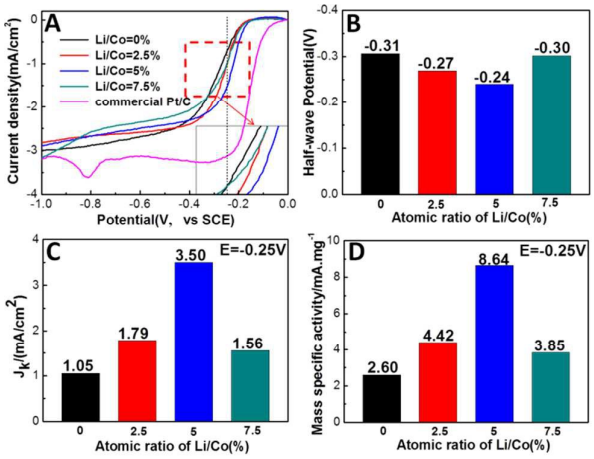

Figure 8. (A) Rotating disk electrode voltammograms of these $Li_xCo_{3-x}O_4$/C fabricated at different Li/Co atomic ratios (0, 2.5%, 5%, 7.5%), compared with a commercial Pt/C (20 wt% of Pt, relative to carbon, E-TEK) at a fixed rotation rate of 1600 rpm in oxygen-saturated 1M NaOH electrolyte at a scan rate of 5 mV/s; (B) The half-wave potential; (C) The oxygen reduction reaction kinetics current density obtained at -0.25V; (D) The mass-specific activities of these $Li_xCo_{3-x}O_4$/C samples obtained at -0.25V.

From Figure 8B, the electro-catalytic activities of these tested catalysts are estimated from the half-wave potential, following the order 5%> 2.5%> 7.5%> 0% with potential values of -0.24, -0.27, -0.30, -0.31V versus a saturated calomel electrode(SCE), respectively. All half-wave potential of the Li-doped Co_3O_4/C (Li/Co=2.5%, 5%, 7.5%) catalysts are more positive than that of undoped Co_3O_4/C catalyst. Among all tested $Li_xCo_{3-x}O_4$/C catalysts, the catalyst fabricated at the Li/Co atomic ratio of 5% clearly exhibits the most positive half-wave potential, which is 70mV higher than the Co_3O_4/C, revealing higher activity for the ORR. Because the half-wave potential is an indicator of ORR activity but is not the truest measure of electrocatalytic activity for ORR, it is general to take another method that is the kinetic current density (J_k), which is related to the intrinsic activity of these catalysts. The kinetic current density (J_k) is obtained by correcting the measured current density according to the Koutecky-Levich equation:

$$\frac{1}{J} = \frac{1}{J_k} + \frac{1}{J_L} = \frac{1}{J_k} + \frac{1}{0.62nFC_0D_0^{2/3}v^{-1/6}\omega^{1/2}} \quad (1)$$

Where J is the measured current density from Figure 8A, J_L is the diffusion-limiting, J_k is the kinetic current, n is the number of electron transferred, F is the Faraday constant (F=96485 C/mol), C_0 is the bulk concentration of O_2 in 1M NaOH (0.843×10^{-6}mol/cm^3) , D_0 is the diffusion coefficient of oxygen in 1M NaOH (1.43×10^{-5} cm^2/s), v is the kinematic viscosity of the electrolyte (0.01128cm^2/s), and ω is the angular velocity. Then the kinetic current is calculated based on the following equation:

$$J_k = \frac{J\times J_L}{J_L - J} \quad (2)$$

As shown in Figure8C, at a given potential of -0.25V, as expected, the ORR kinetic current density (J_k) generated on these Li-doped Co_3O_4/C catalysts are higher than the pure Co_3O_4/C catalyst and the kinetic current densities (J_k) of these catalysts show a volcano plot as a function of Li contents, where the catalyst with 5% Li content locates at the peak. The measured ORR kinetic current density (J_k) of the catalyst is 3.50 mA/cm^2, which is approximately 3.3 times higher than that of the Co_3O_4/C. These results of the half-wave potential and kinetic current densities (J_k) reveal that the ORR activities of these $Li_xCo_{3-x}O_4$/C catalysts exhibit significantly improved electrocatalytic activity for the ORR, compared with pure Co_3O_4.

In order to elucidate the impact of Li content on the ORR kinetics, we plot the mass-specific activity of these $Li_xCo_{3-x}O_4$/C samples as a function of the atomic ratio of Li/Co using the data in Figure 8C, as shown in Figure 8D.[46] We can see that all the $Li_xCo_{3-x}O_4$/C catalysts prepared at the Li contents ranging from 2.5% to 7.5% exhibited better mass-specific activity than the pure Co_3O_4/C. A similar volcano plot of mass-specific activity as a function of Li content in these synthesized $Li_xCo_{3-x}O_4$/C catalysts has been observed here. In this plot, the catalyst fabricated at a Li/Co atomic ratio of 5% displays the highest mass-specific activity (8.64 mA/mg^{-1}), which is also approximately 3.3 times higher than that of the Co_3O_4/C. This finding indicates that the integration of Li element can substantially improve the mass-specific activity of the doped Co_3O_4 effectively, although the mass-specific activity of the pure Co_3O_4 alone is low. Therefore, based on the analysis of the electrochemical measurements such as half-wave potential, kinetic current densities (J_k), and mass-specific activity for the Li-doped Co_3O_4/C catalysts during the ORR, it is concluded that the Li doping can remarkably improve the electrocatalytic activity of Co_3O_4 effectively. More importantly, the electrocatalytic activity of these $Li_xCo_{3-x}O_4$/C samples is corresponding to the XPS results. This illustrates that the increasing amount of the O=C-O-Co^{III}-O bond between the $Li_xCo_{3-x}O_4$ and the carbon black has a substantial impact on the ORR kinetics. Therefore, in this page, we deduce that the excellent performance of these $Li_xCo_{3-x}O_4$/C hybrid catalysts probably results from the enhanced synergistic interaction (O=C-O-Co^{III}-O) at the interface between Li-doped Co_3O_4 nanocrystals and carbon support in these hybrids.

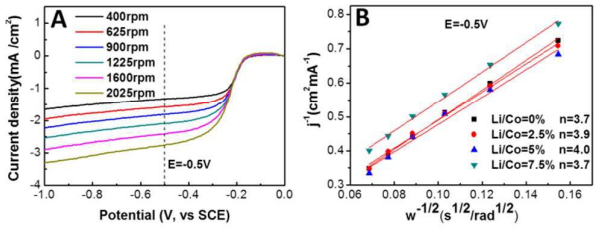

Figure 9. (A) Rotating disk electrode voltammograms of the $Li_xCo_{3-x}O_4$/C sample fabricated at the Li/Co atomic ratio of 5% at various rotation speeds at a scan rate of 5 mV/s ; (B) Koutecky-levich plots (J^{-1} versus $\omega^{-1/2}$) for ORR on these $Li_xCo_{3-x}O_4$/C samples fabricated at different Li/Co atomic ratios (0, 2.5%, 5%, 7.5%) obtained at -0. 5V.

Based on the data of rotating disk electrode measurements at different rotation speeds for these $Li_xCo_{3-x}O_4$/C hybrids shown in Figure 9A, the well-known Koutecky-levich equation (Equation (1)) is employed to determine the numbers of electrons transferred per O_2 molecule (n) in the ORR catalyzed by these catalysts. At a fixed polarization potential of -0.5V vs. SCE, the obtained Koutecky-levich plots (J^{-1} versus $\omega^{-1/2}$) for these $Li_xCo_{3-x}O_4$/C samples are shown in Figure 9B. Thus, the numbers of electrons transferred in ORR on each catalyst is calculated from the slope of its Koutecky-levich plot shown in Figure 9B. As observed, for these $Li_xCo_{3-x}O_4$/C samples prepared at Li/Co atomic ratio of 0%, 2.5%, 5%, 7.5%, the calculated number of transfer electrons is 3.7, 3.9, 4.0 and 3.7, respectively. It indicates that the ORR catalyzed by these $Li_xCo_{3-x}O_4$/C catalysts proceeds mainly through the four-electron pathway. Among these catalysts, the $Li_xCo_{3-x}O_4$/C (Li/Co=5%) catalyzes the ORR undergoing via nearly completely four-electron pathway and produced less HO_2^-. Therefore, the incorporation of Li into Co_3O_4 matrix facilitates the ORR activity and improves the efficiency of the ORR.

Besides their activity toward ORR, long-term durability is another key performance for these catalysts, from the view of practical application. Herein, we performed chronoamperometric measurement in O_2-saturated 1M NaOH solution in order to evaluate the durability of the $Li_xCo_{3-x}O_4$/C (Li/Co=5%) catalyst. Since the commercial Pt/C catalyst (20 wt% of Pt, E-TEK) has been regarded as one of the best catalyst for ORR, it was selected as a reference during the long-term durability measurement under the same operation condition. As shown in Figure 10, at a given polarization potential of -0.3V versus SCE, the chronoamperometric response of the commercial Pt/C catalyst exhibits a sharp decrease with a current retention of approximately 78.9% after 24h. The decline of durability for the Pt-based catalysts is known to gradually attenuate over time by reason of surface oxides, particle dissolution and aggregation, especially in alkaline electrolyte used for alkaline fuel cells.[47] In contrast, the $Li_xCo_{3-x}O_4$/C sample exhibits a very slow attenuation with a high current retention (92.4%) even after 24h. These results clearly reveal that the active sites on $Li_xCo_{3-x}O_4$/C catalyst are much more stable than the active sites on the Pt/C catalyst. Since the lack of catalyst durability is one of the major challenges for alkaline fuel cells by now, the excellent stability of our $Li_xCo_{3-x}O_4$/C catalyst make it a promising inexpensive cathodic electrocatalyst for ORR and other important catalytic reactions in alkaline solutions.

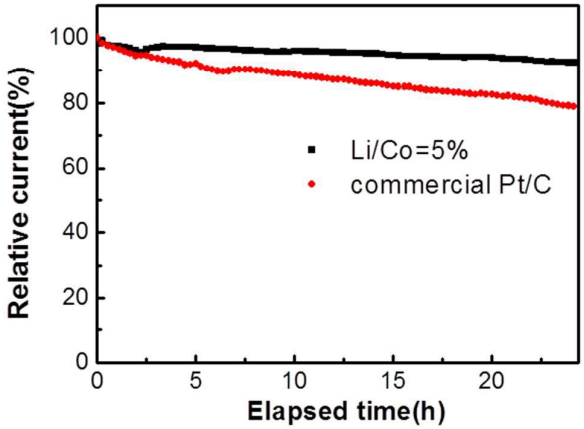

Figure 10. Chronoamperometric responses of $Li_xCo_{3-x}O_4$/C sample (Li/Co=5%) and commercial Pt/C (20 wt% of Pt, relative to carbon, E-TEK) catalyst in O_2-saturated 1M NaOH solution at -0.3 V and 900 rpm.

3.4 Analysis of the improved ORR kinetics over this hybrid.

In this work, we deeply explore the ORR kinetics in detail, based on the formation of the covalent $O{=}C{-}O{-}Co^{III}$ bonds between the doped Co_3O_4 nanoparticles and carbon black in this $Li_xCo_{3-x}O_4$/C catalyst (Li/Co=5%). As we mentioned in Figure 9, the ORR catalyzed by these $Li_xCo_{3-x}O_4$/C electrocatalysts proceeds mainly through the four-electron pathway and the incorporation of Li improved the numbers of electrons transferred per O_2 molecule (n) in the ORR. And among these catalysts, the $Li_xCo_{3-x}O_4$/C (Li/Co=5%) catalyzes the ORR undergoing via nearly completely four-electron pathway and produced less

HO_2^-. This conclusion is in agreement with the results available in the literature. [48-50]Considering the improved ORR activity of the hybrid catalyst observed in Figure 8, a possible mechanism for the ORR kinetics followed a four-electron transfer pathway can be explained by the following four stages: [48-50]

Stage1: surface hydroxide displacement as

$$O{=}C{-}O{-}Co^{III}{-}OH^- + O_2 + e^- \rightarrow O{=}C{-}O{-}Co^{IV}{-}OO^{2-} + OH^- \quad (3)$$

Stage 2: surface peroxide formation as

$$O{=}C{-}O{-}Co^{IV}{-}OO^{2-} + H_2O + e^- \rightarrow O{=}C{-}O{-}Co^{III}{-}OOH^- + OH^- \quad (4)$$

Stage 3: surface oxide formation as

$$O{=}C{-}O{-}Co^{III}{-}OOH^- + e^- \rightarrow O{=}C{-}O{-}Co^{IV}{-}O^{2-} + OH^- \quad (5)$$

Stage 4: surface hydroxide regeneration as

$$O{=}C{-}O{-}Co^{IV}{-}O^{2-} + H_2O + e^- \rightarrow O{=}C{-}O{-}Co^{III}{-}OH^- + OH^- \quad (6)$$

The overall process of ORR above catalysed by the hybrid catalyst is presented in Figure 11A. During the process of the surface hydroxide displacement (Stage 1), the dissolved oxygen molecules (O_2) in the electrolyte can gain one electron from the employing cathodic current and an another electron from the redox of Co^{III}/Co^{IV} and then reduces into a OO^{2-} specie adsorbed on the surface of the Co^{IV} ion. At the same time, the surface-absorbed hydroxides (OH^-) adsorbed on the original Co^{III} ion can be displaced by the OO^{2-} specie and release into the electrolyte. It is believed that the reaction of surface hydroxide displacement (stage 1) is the rate-limiting step of the ORR in alkaline solutions. [50, 51]In our case, since the O=C–O group existed in the O=C–O–Co^{III}–O bond is electron-withdrawing group, it can lead to positively charged Co^{III} ion in this bond above. As a result, this positively charged Co^{III} ion is easily oxidized by the dissolved oxygen to generate Co^{IV} and OO^{2-} species respectively, which substantially promote the reaction of surface hydroxide displacement (Stage 1). During the step of the surface peroxide formation (Stage 2), the formed OO^{2-} specie subsequently react with a water molecule in the electrolyte to produce OOH^- specie, which can absorb onto the surface of Co^{III} derived from the electrochemical reduction of Co^{IV} in the O=C–O–Co^{IV}–O bond. During the surface oxide formation (Stage 3), the Co^{III} be oxidized into the Co^{IV} once again, following breaking of the O–O bond in the surface peroxide (OOH^-) and forming of surface oxide (O^{2-}) that absorbs onto the surface of Co^{IV} ion. Similar to the Stage 1, the Co^{III} is easily oxidized into the Co^{IV} due to the presence of O=C–O group in the O=C–O–Co^{III}–O bond, which also contribute the reaction at Stage 3. At stage 4 (the surface hydroxide regeneration), the Co^{IV} is electrochemically reduced into the Co^{III} once again, accompanying that the surface oxide (O^{2-}) reacts with a water molecule to produce a surface hydroxide that adsorbs onto the surface of the reduced Co^{III} ion. In this way, the overall oxygen reduction process catalysed by the hybrid would follow the whole cycle in Figure 11A and each cycle can consume 4 electrons, a dissolved oxygen(O_2) and $2H_2O$ to produce $4OH^-$ that release into the electrolyte, through a fully four-electron pathway.

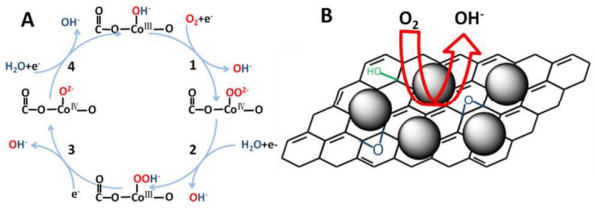

Figure 11. (A) The ORR kinetics mechanism of $Li_xCo_{3-x}O_4$ /C catalyst in alkaline environments (B) The overall ORR process catalysed by this hybrid.

Therefore, based on the analysis of the ORR kinetics in detail in Figure 11A, we can conclude that the formation of the covalent O=C–O–Co^{III}–O bonds at the interface between Co_3O_4 nanocrystals and the carbon support in their hybrid remarkably facilitate the ORR kinetics, where Co^{III} ions in the O=C–O–Co^{III} –O bonds are the active sites for the ORR. Moreover, compared with the undoped Co_3O_4/C, the incorporation of Li ions into Co_3O_4 lattice can significantly increase the amount of the O=C–O–Co^{III}–O bond in the $Li_xCo_{3-x}O_4$/C catalyst, as evidenced by the results from the XPS analysis (Figure 4, 5). The increased amount of the O=C–O–Co^{III}–O bond would accelerate the rate of surface hydroxide displacement, that is, a rate-limiting step of the ORR in alkaline environments. Therefore, based on the proposed mechanism of the ORR above, the chemical coupling of the oxide nanoparticles with carbon is responsible for the enhanced ORR electrocatalytic activity of the $Li_xCo_{3-x}O_4$/C hybrid catalyst. The overall ORR process occurs at the interfaces formed by the doped Co_3O_4 nanocrystals and their carbon support in this hybrid, as shown in Figure 11B.

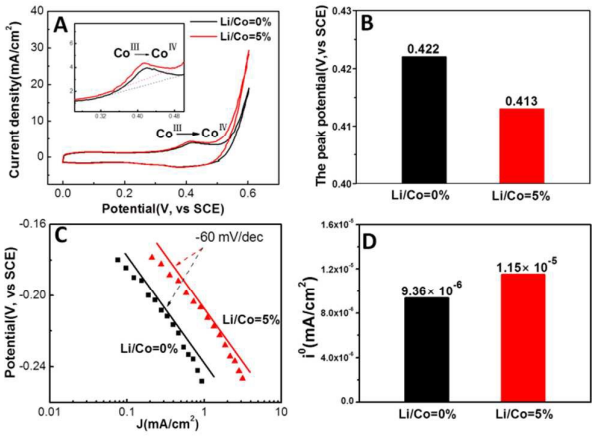

Figure 12. (A) Cyclic voltammograms of these $Li_xCo_{3-x}O_4$/C samples fabricated at the Li/Co atomic ratios of 0% and 5% in 1M NaOH at scan rate of 50mV/s; (B) The peak potential of the Co^{3+} oxidation peaks of these two samples

In order to confirm the enhanced synergistic interaction for $Li_xCo_{3-x}O_4$/C catalysts, we have conducted the cyclic voltammogram (CV) measurements for the $Li_xCo_{3-x}O_4$/C (Li/Co=5%) and undoped Co_3O_4/C (Li/Co=0%) catalysts, and the obtained results are depicted in Figure 12A. As observed in Figure 12A, similar to the Co_3O_4/C, there is a pair of redox peaks ($Co^{\square}/^{\square}$) is observed for the $Li_xCo_{3-x}O_4$/C catalyst. The corresponding oxidation peak (at around 0.45V) is assigned to the oxidation of the $Co^{\square}$ to $Co^{\square}$ ions for these two catalysts. [21] For the Li-doped catalyst, however, the corresponding peak potential of the $Co^{\square}$ oxidation is slightly negatively shifted, relative to that of the undoped sample, as shown in Figure 12B. Moreover, the recorded peak current of the $Co^{\square}$ oxidation for the doped catalyst is obviously higher than that of Co_3O_4/C shown in Figure 12A. These outcomes illustrate that the $Co^{\square}$ ions in the $Li_xCo_{3-x}O_4$/C catalyst are much easier to be oxidized to $Co^{\square}$ than those in the Co_3O_4/C. Since the O=C–O group existed in the O=C–O–$Co^{\square}$–O bond is electron-withdrawing group, the easier oxidation of the $Co^{\square}$ into $Co^{\square}$ ions results from the formation of increased O=C–O–$Co^{\square}$–O bonds formed at the interface between Li-doped Co_3O_4 nanocrystals and carbon support in the doped catalyst with respect to the undoped catalyst. The small negative shift of the redox peak potential for the $Co^{III/IV}$ pair is attributed to the fact that the amount of Co^{3+} ions in the O=C-O-Co^{III}-O bonds formed at the interface is small, relative to most of Co^{3+} ions existed in bulk Co_3O_4 matrix. Thus, the promoted oxidation of the Co^{III} into Co^{IV} ions in the $Li_xCo_{3-x}O_4$/C catalyst further confirms the presence of the enhanced synergistic interaction as a result of increased O=C–O–Co^{III}–O bonds formed at the interface between the Li-doped Co_3O_4 and carbon in the $Li_xCo_{3-x}O_4$/C catalyst. As suggested by Figure 11, the enhanced covalent O=C–O–$Co^{\square}$–O bonds can promote OO^{2-} specie adsorption and surface hydroxide displacement on the Co ions, that is, the rate-limiting step of the ORR on the Li-doped catalyst in alkaline solutions (Step 1).

To further verify the enhanced synergistic interaction (O=C-O-$Co^{\square}$-O) at the interface between Li-doped Co_3O_4 nanocrystals and carbon support in these hybrids is responsible for the improved ORR activity, we constructed Tafel plots for the $Li_xCo_{3-x}O_4$/C (Li/Co=5%) and Co_3O_4/C (Li/Co=0%) samples, as shown in Figure 12C. As observed, under low overpotential condition, a similar Tafel slope of 60 mV dec^{-1} is observed for two samples. Based on the data in Figure 12C, the exchange current density in the ORR is further determined for each sample by using the Tafel equation:

$$E - E^0 = -b \log i^0 + b \log i \qquad (7)$$

Where E^0 is the equilibrium potential of ORR, b in the Tafel slope and i^0 is the exchange current density. The obtained value of the exchange current density for each sample is shown in Figure 12D. As expectedly, the $Li_xCo_{3-x}O_4$/C (Li/Co=5%) catalyst exhibits a much higher exchange current density than that of the Co_3O_4/C, which implies its ability to accelerate the rate-determining step (Step1) during the ORR.[46] This finding confirms the fact that the enhanced synergistic interaction due to increased O=C–O–$Co^{\square}$–O bonds formed in the catalyst is responsible for the improved ORR activity of $Li_xCo_{3-x}O_4$/C catalyst.

4. Conclusions

This synthesis method provided a hydrothermal route to prepare the $Li_xCo_{3-x}O_4$ solid solution integrated on the carbon via the in-situ nucleation and growth of the mixed metal oxide on carbon. The carbon supports $Li_xCo_{3-x}O_4$ spinel nanocrystals with average particle size of approximately 4 nm, covered evenly on the surface of carbon in this hybrid. The incorporation of the Li promotes the formation of the O=C–O–Co^{III}–O bonds at the interfaces between oxide and carbon support in this hybrid series, where the highest content of this bond is observed for the sample prepared at the Li/Co atomic ratio of 5%. The formation of the unique covalent bonds contributes the ORR electro-catalytic activity in our case. The ORR electro-catalytic activity of these catalysts shows a volcano plot as a function of Li contents, where the catalyst with 5% Li content locates at the peak. Moreover, the $Li_xCo_{3-x}O_4$/C catalyst exhibits a better long-term durability than the commercial Pt/C catalyst (20 wt% of Pt, E-TEK). The ORR of the $Li_xCo_{3-x}O_4$/C catalyst proceeds via four stages, and the increase of the unique covalent bonds (O=C–O–Co^{III}–O) accelerates the rate of surface hydroxide displacement(Stage 1), that is, the rate-limiting step of the ORR in alkaline environments. Therefore, the construction of the hybrid catalysts with the unique interface structure may open up more ways to develop other carbon-supported alkali metal-doped Co_3O_4 as catalysts for ORR to meet the increasing application demand.

Acknowledgements

This work was supported by the National Natural Science Funds of China (Grant No. 51272018, 51125007)

References

1 F. Cheng, J. Shen, B. Peng, Y. Pan, Z.Tao and J. Chen, *Nat. chem.*, 2011, 3, 79-84
2 W H. Bragg, *Nature*, 1915, 95, 561.
3 X. Xie, Y. Li, Z. Q. Liu, M. Haruta and W.Shen, *Nature*, 2009, 458, 746-749.
4 Y. Liang, H. Wang, J. Zhou, Y. Li, J. Wang, T. Regier and H. Dai, *J. Am. Chem. Soc.*, 2012, 134, 3517-3523.
5 Y. Liang, Y. Li, H. Wang, J. Zhou , J. Wang, T. Regier and H. Dai, *Nat. mater.*, 2011, 10, 780-786
6 J. Feng, Y. Liang, H. Wang, Y. Li, B. Zhang, J. Zhou, T. Regier and H. Dai, *Nano Res.*, 2012, 5, 718-725.
7 L. Li, S. Liu, A. Manthiram, *Nano Energy*, 2015, 12, 852–860.
8 L. T. Anh, A. K. Rai, T. V.Thi, J. Gim, S. Kim, V. Mathew and J. Kim, *J. Mater. Chem. A*, 2014, 2, 6966-6975.
9 F. Bidault, D. J. L. Brett, P. H. Middleton and N. P. Brandon, *J. Power Sources*, 2009, 187, 39–48.
10 L. Wang, B. Liu, S. Ran, H. Huang, X. Wang, B. Liang and G. Shen, *J. Mater. Chem.*, 2012, 22, 23541-23546.
11 M. Hamdani, R. N. Singh and P. Chartier, *Int. J. Electrochem. Sci*, 2010, 5, 556.
12 X. Wu and K. Scott, *Int. J. Hydrogen Energ.*, 2013, 38, 3123-3129.
13 F. Švegl, B. Orel, I. Grabec-Švegl and V. Kaučič, *Electrochim. Acta*, 2000, 45, 4359-4371.
14 C. Bocca, G. Cerisola, E. Magnone and A. Barbucci, *Int. J. Hydro. Energy*, 1999, 24(8): 699-707.
15 K. Asano, C. Ohnishi, S. Iwamoto, Y. Shioya, and M. Inoue, *Appl. Catal. B: Environ.* , 2008, 78, 242-249
16 M. Sun, L. Wang, B. Feng, Z. Zhang, G. Lu, and Y. Guo, *Catal. Today*, 2011, 175, 100-105.
17 M. De Koninck, S.C. Poirier and B. Marsan, *J. Electrochem. Soc.*, 2007, 154, A381-A388.
18 M. De Koninck and B. Marsan, *Electrochim. Acta*, 2008, 53, 7012-7021.
19 H. Liu, J. Liu, W. Song, F. Wang and Y. Song, *Mater. Lett.*, 2015, 139, 447-450.
20 T. Maiyalagan, K.A. Jarvis, S. Therese, P.J. Ferreira, A. Manthiram, *Nat. Commun.*, 2014, 5, 536-538.
21 J. Xu, P. Gao and T.S. Zhao, *Energ. & Environ. Sci.*, 2012, 5, 5333-5339.
22 J. Suntivich, H. A. Gasteiger, N. Yabuuchi, H. Nakanishi, J. B. Goodenough and Y. Shao-Horn, *Nat. chem.*, 2011, 3, 546-550.
23 G. Liu, , X. Li, , P. Ganesan and B. N. Popov, *Appl. Catal. B: Environ.*, 2009, 93, 156-165.
24 Y. Zhao, L. Yang, S. Chen, X. Wang, Y. Ma, Q. Wu, Y. Jiang, W. Qian and Z. Hu, *J. Am. Chem. Soc.*, 2013, 135, 1201-1204.
25 H. Wang, H. Dai, *Chem. Soc. Rev.*, 2013, 42, 3088-3113.
26 J. Xiao, G. Xu, S. G. Sun and S. Yang, *Part. Syst. Charact.*, 2013, 30, 893-904.
27 L. He, Z. Li and Z. Zhang, *Nanotechnology*, 2008, 19, 155606.
28 X. Wang, J. Xu, X. Yu, K. Xue, J. Yu and X. Zhao, *Appl. Phys. Lett.*, 2007, 91, 031908.
29 P. Rasiyah and A.C.C. Tseung, *J. Electrochem. Soc.*, 1983, 130, 365-368.
30 I. Nikolov, R. Darkaoui, E. Zhecheva, R. Stoyanova, N. Dimitrov and T. Vitanov, *J Electroanal Chem.*, 1997, 429, 157-168.

31 J. Liu, X. Jin, W. Song, F. Wang, N Wang and Y Song, *Chin. J. Catal.*, 2014, 35, 1173-1188.
32 J. F. Marco, J. R. Gancedo, M. Gracia, J. L. Gautier, E. Rí and F. J. Berry, *J. Solid State Chem.*, 2000, 153, 74-81.
33 S. Xiong, J. S. Chen, X. W. Lou and H. C. Zeng, *Adv. Funct. Materials*, 2012, 22, 861-871.
34 L. Li, Y. Li, S. Gao, and N. Koshizaki, *J. Mater.Chem.*, 19, 8366-8371.
35 J. Park, G.P. Kim, H.N. Umh, I. Nam, S .Park, Y. Kim and J. Yi, *J. Nanopart. Res.*, 2013, 15, 1-9.
36 G. He, J. Li, H. Chen, J. Shi, X. Sun, S. Chen and X. Wang, *Mater. Lett.*, 2012, 82, 61-63.
37 M. Burriel, G. Garcia, J. Santiso, A. Abrutis, Z. Saltyte, and A. Figueras, *Chem. Vapor Depos.*, 2005, 11, 106–111.
38 J.L. Gautier, E. Rios, M. Gracia, J.F. Marco and J.R. Gancedo, *Thin Solid Films*, 1997, 311, 51-57.
39 J.F. Marco, J.R. Gancedo, M. Gracia, J.L. Gautier, E. Rí and J.F. Berry, *J. Solid State Chem.*, 2000, 153, 74-81.
40 A. Restovic, E. Rıos, S. Barbato, J. Ortiz and J.L. Gautier, *J. Electroanal. Chem.*, 2002, 522, 141-151
41 F. Avilés, J. V. Cauich-Rodríguez, L. Moo-Tah, A. May-Pat and R. Vargas-Coronado, Carbon, 2009, 47, 2970-2975.
42 D. B. Mawhinney, V. Naumenko, A. Kuznetsova, J. T. Yates, J. Liu and R. E. Smalley, J. Am. Chem. Soc., 2000, 122, 2383-2384.
43 Y. Z. Wang, Y. X. Zhao, C. G. Gao and D. S. Liu, Catalysis Letters, 2007, 116, 136-142.
44 Y. Shao, G. Yin, J. Zhang and Y. Gao, Electrochim. Acta, 2006, 51, 5853-5857.
45 J. Wang, G. Yin, Y. Shao, S.Zhang, Z. Wang and Y. Gao, J. Power sources, 2007, 171, 331-339.
46 Y. Zhao, J. Liu, Y. Zhao and F. Wang, *Phys. Chem. Chem. Phys.*, 2014, 16, 19298-19306.
47 W. Jin, H. Du, S. L. Zheng, H. B. Xu and Y. Zhang, *J. Phys. Chem.*, 2010, 114, 6542–6548.
48 Y. Matsumoto, H. Yoneyama and H. Tamura, *J. Electroanalytical Chem. Inter. Electrochem.*, 1977, 83, 237-243.
49 J. Suntivich, H.A. Gasteiger, N. Yabuuchi, H. Nakanishi, J. B. Goodenough and Y. Shao-Horn, *Nat. Chem.*, 2011, 3, 546-550.
50 Y. Wang and H. P. Cheng, *J. Phys. Chem. C*, 2013, 117, 2106-2112.
51 Z. Wang, D. Xu, J. Xu and X. Zhang, *Chem. Soc. Rev.*, 2014, 43, 7746-7786.